PHYSICAL REVIEW B **90**, 081406(R) (2014)

High-Chern-number bands and tunable Dirac cones in β-graphyne

Guido van Miert, Cristiane Morais Smith, and Vladimir Juričić
Institute for Theoretical Physics, Centre for Extreme Matter and Emergent Phenomena, Utrecht University, Leuvenlaan 4, 3584 CE Utrecht, The Netherlands

(Received 19 May 2014; revised manuscript received 9 August 2014; published 25 August 2014)

Graphynes represent an emerging family of carbon allotropes that recently attracted much interest due to the tunability of the Dirac cones in the band structure. Here, we show that the spin-orbit couplings in β-graphyne could produce various effects related to the topological properties of its electronic bands. Intrinsic spin-orbit coupling yields high- and tunable Chern-number bands, which may host both topological and Chern insulators, in the presence and absence of time-reversal symmetry, respectively. Furthermore, Rashba spin-orbit coupling can be used to control the position and the number of Dirac cones in the Brillouin zone. These findings suggest that spin-orbit-related physics in β-graphyne is very rich, and, in particular, that this system could provide a platform for the realization of a two-dimensional material with tunable topological properties.

DOI: 10.1103/PhysRevB.90.081406 PACS number(s): 73.22.−f, 31.15.aj, 31.15.ae

Introduction. Since its synthesis in 2004, graphene has attracted enormous attention due to its unusual properties, and has provided a new paradigm for Dirac materials in condensed-matter physics [1]. Unconventional electronic properties in this material arise as a consequence of the pseudorelativistic nature of its low-energy quasiparticles. Furthermore, graphene represents a platform for the first proposed time-reversal invariant topological insulator [2], which, however, has not been realized experimentally due to a weak spin-orbit coupling (SOC). Since then, achieving strong SOC in Dirac materials has been one of the goals that motivated the search for alternatives to graphene, and promising candidates have been recently proposed, including self-assembled honeycomb arrays of heavy-atom semiconducting nanocrystals, such as Pb and Se [3], patterned quantum dots [4], and molecular graphene [5]. An important new emerging class of two-dimensional (2D) carbon allotropes consists of graphynes, among which the most studied members include α-, β-, and γ-graphynes [6]. They have not been synthesized yet, in contrast to the structurally similar graphdiyne, which has been recently fabricated [7], but first steps towards that goal have been achieved [8,9].

Graphynes are allotropes of carbon obtained by inserting a triple bond (−C≡C−) into the graphene structure; see Fig. 1(a). These 2D allotropes of carbon were proposed in 1987 [10], and their structural, electronic, and mechanical properties have been rather extensively studied [11–17]. They have recently attracted much interest, especially because of the existence of tunable Dirac cones in their band structure, and in that sense could be even more promising for applications than graphene [18,19]. Features of the Dirac cones may be controlled by chemical reactions [20] and adatoms [21–23]. Adatoms of heavy elements, such as indium and thallium, could also be used to tune SOC in graphynes, as suggested in Ref. [24] for graphene, which is particularly important in light of inducing and manipulating topological properties, critically dependent on its strength.

Motivated by these developments, in this Rapid Communication we study the effects of the SOCs in β-graphyne [(Fig. 1(a)], and show that this material could be advantageous with respect to graphene not only concerning the tunability of the Dirac cones [18] but also regarding topological properties of its band structure. To do so, we derive an effective tight-binding (TB) theory that includes both Rashba and intrinsic SOCs. So far, their effects have been only sparsely studied using *ab initio* methods [25], but clearly an effective description of the SOCs in graphynes is highly desirable. Before elaborating on the specific results, we first observe that due to the lattice structure of β-graphyne, a minimal effective TB model contains six low-energy p_z orbitals, one on each of the six sites on the vertices within the unit cell. Second, for either of the two types of SOC there are, in fact, two parameters, which we call *internal* and *external*, describing the corresponding intra- and inter-unit-cell hoppings. In graphene, these two parameters are equal, since intra- and inter-unit-cell bonds therein are equivalent. This fact in conjunction with the larger unit cell (18 atoms in β-graphyne versus two in graphene) already hints that the SOC-related physics in β-graphyne could be richer than in graphene.

Indeed, this is the case. Without SOCs, there are six *inequivalent* Dirac cones at the Fermi level along the high-symmetry Γ-M line in the Brillouin zone (BZ) [Fig. 1(b)]. As the internal Rashba SOC is cranked up, we show that the system undergoes a series of Lifshitz phase transitions in which the Dirac cones split, merge, and split again, however, in different directions in the BZ (Fig. 2). The effect of the intrinsic SOC, on the other hand, is to produce gapped topologically nontrivial bands with *tunable* Chern numbers as high as $C = 4$ per spin (Fig. 3), suggesting that β-graphyne could provide the ground for realizing both conventional (noninteracting) and fractional topological insulators upon accounting for interactions [26]. In fact, as we show here, various topologically insulating phases may emerge at half filling both in the presence and in the absence of time-reversal symmetry (TRS), demonstrating the possibility of achieving topological phase transitions in a carbon-based material.

Tight-binding description of the SOC. Among the three most studied graphynes, β-graphyne has the most complicated lattice structure. Its unit cell consists of a hexagon, which has one carbon atom located at each vertex, and two carbon atoms connected by an acetylene linkage between each two neighboring vertices, yielding together 18 atoms; see Fig. 1(a). For the description of SOC effects, we use a basis that contains two sets of orbitals: σ orbitals, consisting of the atomic s, p_x,

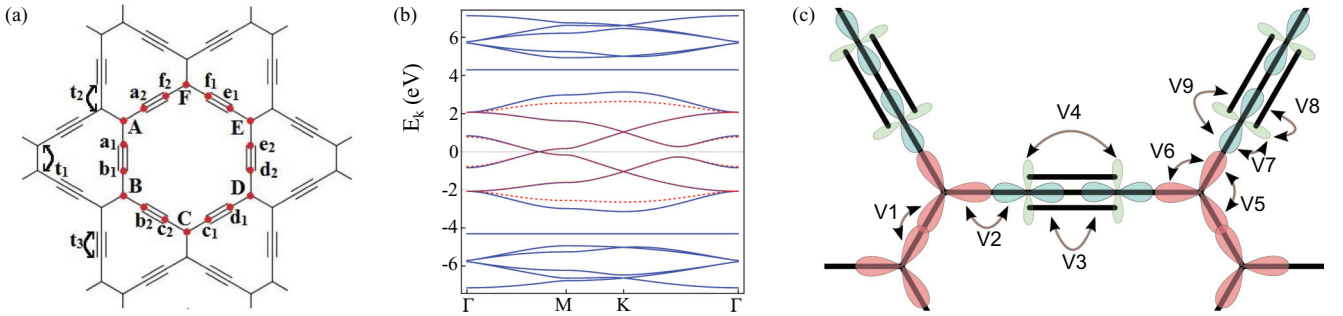

FIG. 1. (Color online) (a) Lattice structure of β-graphyne together with NN hopping parameters for p_z orbitals t_i ($i = 1,2,3$). (b) Band structures along high-symmetry lines obtained from the full 18-orbital p_z-TB model and from the effective six-orbital p_z-TB model, shown in blue (solid) and red (dashed) lines, respectively, with Fermi level at zero energy. (c) Hopping parameters (V_j, $j = 1,\ldots,9$) used in the TB model describing the σ orbitals with the red, blue, and green colors labeling sp^2, sp, and p orbitals, respectively.

and p_y orbitals, as well as p_z orbitals. To obtain an effective Hamiltonian containing only six p_z orbitals at the vertices, we proceed in two steps: (i) we first integrate out high-energy σ orbitals to obtain a Hamiltonian with 18 p_z orbitals at both vertex and edge sites in the unit cell; (ii) in the second step, we eliminate 12 p_z orbitals at the edge sites.

We first analyze the system without SOC, when the σ and p_z orbitals are decoupled, and only the latter are relevant for the low-energy description at half filling. The corresponding band structure is displayed in Fig. 1(b) (blue solid lines). Using step (ii) in the outlined procedure, we obtain an effective Hamiltonian with only six p_z orbitals located at the lattice vertices [27]

$$H_z^{\text{eff}} = t_{\text{int}} \sum_{\langle i,j \rangle} [A_i^\dagger (B_j + F_j) + C_i^\dagger (B_j + D_j) + E_i^\dagger (D_j + F_j)] + t_{\text{ext}} \sum_{\langle i,j \rangle} [A_i^\dagger D_j + C_i^\dagger F_j + E_i^\dagger B_j] + \text{H.c.}, \quad (1)$$

with $t_{\text{int}} = -t_2^2 t_3 / T$ and $t_{\text{ext}} = t_1 t_3^2 / T$, denoting nearest-neighbor (NN) intra-unit-cell and inter-unit-cell hoppings, respectively, and $T \equiv 2t_2^2 + t_3^2$. The hopping parameters for the 18 p_z orbitals are [Fig. 1(a)] $t_1 = -2.00$ eV, $t_2 = -2.70$ eV, and $t_3 = -4.30$ eV [27], hence $t_{\text{int}} = 0.95$ eV and $t_{\text{ext}} = -1.12$ eV. It turns out that this Hamiltonian captures the low-energy band structure at half filling very well; see Fig. 1(b) (red dashed lines). Note that the dispersion relation exhibits six Dirac cones at the Fermi level, located on the line Γ-M. As opposed to graphene and α-graphyne, where the cones exhibit a threefold rotational symmetry, in β-graphyne the cones are symmetric only under mirror reflection through the normal plane containing the line Γ-M, and are thus anisotropic [18].

We now turn to the description of the effects arising from both intrinsic and Rashba SOCs with the Hamiltonian

$$H_{\text{SOC}} = H_L + H_E. \quad (2)$$

The intrinsic SOC originates from relativistic effects, microscopically described by the Hamiltonian $H_L = -f(r)\boldsymbol{\sigma} \cdot \mathbf{L}$, where f is a function related to the effective short-ranged nuclear electrostatic potential, $\boldsymbol{\sigma}$ is a vector of Pauli matrices, and $\mathbf{L}$ is the orbital angular momentum. Furthermore, this coupling possesses mirror symmetry through the lattice (x-y) plane, represented by the matrix σ_z in spin space. This symmetry then allows for the coupling between $p_{z,\uparrow}$, $p_{x,\downarrow}$,

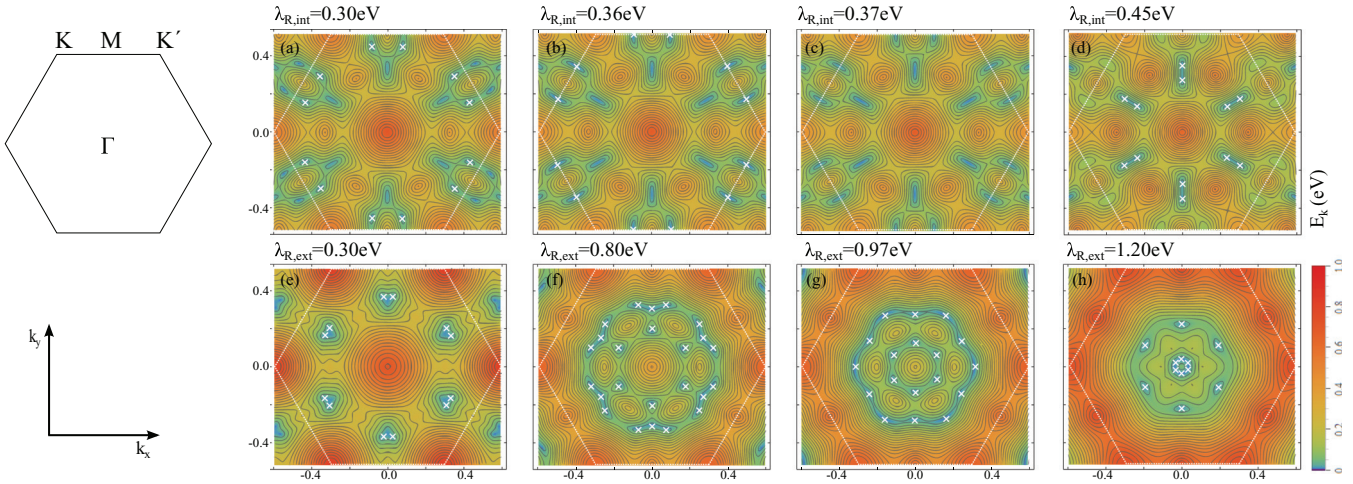

FIG. 2. (Color online) Band structure in the presence of the Rashba SOC for $t_{\text{ext}}/t_{\text{int}} = -1.18$. The panels in the upper (lower) row display the Lifshitz transitions driven by the internal (external) Rashba SOC. The BZ is represented by a white line; the Dirac cones are labeled by white crosses in the plots. The high-symmetry points in the BZ are shown in the upper left panel and momentum is in units with the lattice constant set to 1.

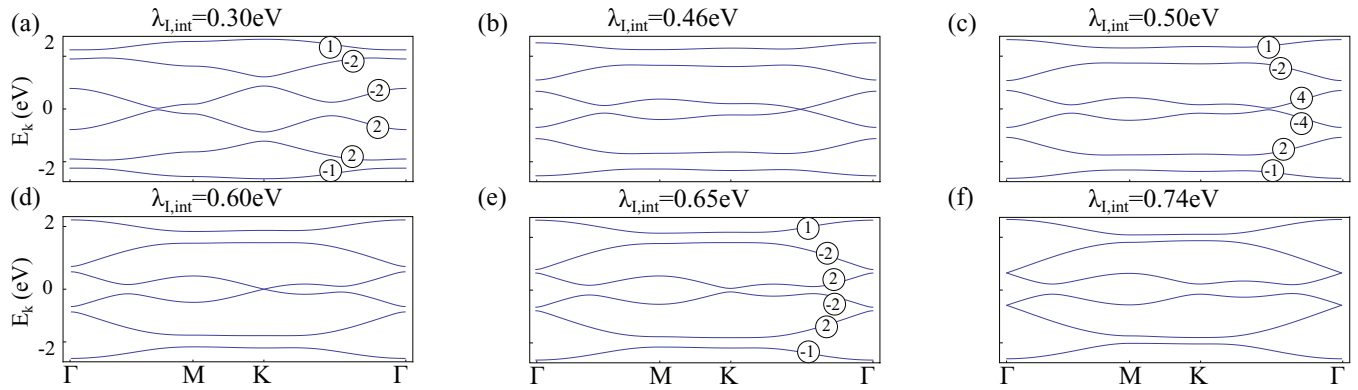

FIG. 3. (Color online) The six panels display the band structure along high-symmetry lines for β-graphyne with the internal intrinsic SOC. The numbers in the circles denote the Chern numbers for the respective bands with spin up.

$p_{y,\downarrow}$, and $s_\downarrow$ orbitals, odd under this reflection. Analogously, the orbitals $p_{z,\downarrow}$, $p_{x,\uparrow}$, $p_{y,\uparrow}$, and $s_\uparrow$, even under this symmetry, can be coupled. Moreover, when an external electric field is applied perpendicularly to the plane, the microscopic Hamiltonian includes an extra term $H_E = Ez$, with E the electric field, that couples the s to the p_z orbitals due to the broken mirror symmetry. A linear in E combination of the Hamiltonians H_L and H_E generates the Rashba SOC, whereas the intrinsic SOC is generated exclusively by H_L [28]. In addition to the σ orbitals, in principle, the d_{xz} and d_{yz} orbitals have to be taken into account for SOC [29]. However, the d orbitals are expected not to lead to any qualitatively different effects in β-graphyne, and we do not consider those hereafter [30].

To derive an effective model describing the SOC, we apply the outlined two-step procedure to the Hamiltonian

$$H = H_0^z + H_0^\sigma + H_E^{z,\sigma} + H_L^{z,\sigma} + \left(H_E^{z,\sigma}\right)^\dagger + \left(H_L^{z,\sigma}\right)^\dagger, \quad (3)$$

where H_0^z (H_0^σ) describes hoppings between p_z (σ) orbitals denoted by t_i (V_i) (see Figs. 1(a), 1(c), and Supplemental Material [28]), while the SOC terms, obtained from Eq. (2), read

$$H_E^{z,\sigma} = \sum_{j,\alpha=1,2} \xi_{sp\alpha}\, p_{z,j\alpha}^\dagger s_{j\alpha},$$

$$H_L^{z,\sigma} = \sum_{j,\alpha=1,2} \xi_{p\alpha}\, p_{z,j\alpha}^\dagger (-i\sigma_y p_{x,j\alpha} + i\sigma_x p_{y,j\alpha}).$$

Here, $p_{z,i}^\dagger$ creates an electron in a p_z orbital at position i, and analogous notation is used for the p_x, p_y, and s orbitals, while $\alpha = 1$ (2) corresponds to the sites at edge (vertex). The exact value of the on-site coupling parameters ξ_{p1}, ξ_{p2}, ξ_{sp1}, and ξ_{sp2} may be obtained by fitting the band structure to *ab initio* calculations, which, however, have been performed only for α-, δ-, and 6,6,12- but not for β-graphyne with intrinsic SOC [20]. Note that ξ_{sp1} and ξ_{sp2} are both linear in E. An approximate lower bound for $\xi_{p1} \simeq 12.6$ meV found in α-graphyne may also apply to β-graphyne since the charge distribution around the acetylene bond is approximately the same for all graphynes. To obtain an estimate for ξ_{p2}, we use that the charge distribution around the vertices in β-graphyne and graphene are approximately the same, and therefore we expect that their values should be comparable, yielding $\xi_{p2} \simeq 2.8$ meV [29]. The parameters ξ_{sp1} and ξ_{sp2} should be approximately equal, since they derive from the corresponding matrix elements of the microscopic Hamiltonian H_E for the wave functions at the edges and vertices, expected to be comparable, yielding $\xi_{sp1} \approx \xi_{sp2} \simeq 10$ meV for a typical $E \simeq 0.1$ V/nm [29]. These estimates are, however, expected to be modified in the presence of heavy adatoms and strain. The latter should influence the charge distribution around the edges making it more inhomogeneous, and therefore enhancing the value of the SOC parameters.

The obtained effective Hamiltonian that contains only six p_z orbitals reads

$$H^{\text{eff}} = H_z^{\text{eff}} + H_{\text{R}}^{\text{eff}} + H_{\text{I}}^{\text{eff}}, \quad (4)$$

with H_z^{eff} given by Eq. (1), while the Rashba and the intrinsic SOCs are given, respectively, in terms of NN and next-NN TB Hamiltonians,

$$H_{\text{R}}^{\text{eff}} = i \sum_{a,\langle i,j\rangle} \lambda_{R,a}\, p_{z,i}^\dagger\, (\boldsymbol{\sigma} \times \hat{\mathbf{d}}_{ij}) \cdot \hat{\mathbf{z}}\, p_{z,j}, \quad (5)$$

$$H_{\text{I}}^{\text{eff}} = i \sum_{a,\langle\langle i,j\rangle\rangle} \lambda_{I,a}\, v_{ij}\, p_{z,i}^\dagger\, \sigma_z\, p_{z,j}. \quad (6)$$

Here, the index $a = \text{int}\,(\text{ext})$ refers to the SOCs effectively described by the intra-(inter-)unit-cell hoppings with the summations also taken correspondingly, $\hat{\mathbf{d}}_{ij}$ is a unit vector connecting NNs, and $v_{ij} = +(-)$ if the hopping is (anti-)clockwise. The parameters of the six-band effective SOC Hamiltonian (4), derived from the Hamiltonian (3), are given in Table I.

Effects of the Rashba SOC: Tunable Dirac cones. We first neglect the intrinsic SOC and consider the effects of the internal Rashba SOC, $\lambda_{\text{R,int}}$, since this term is expected to dominate over the external one in β-graphyne. This can be understood from the fact that the internal Rashba SOC arises from the hoppings through the acetylene bond. Since these hoppings yield three times as many possibilities to flip spin as the ones not involving acetylene bonds, which pertain to the external Rashba SOC, the internal Rashba SOC is thus expected to dominate. Indeed, estimates for the microscopic SOC parameters, together with expected similar values for the hoppings between σ orbitals $V_1 \approx V_2 \approx V_3$ ($\simeq$5–10 eV) [29],

TABLE I. Effective Rashba and intrinsic SOC parameters for β-graphyne in Hamiltonians (5) and (6), respectively, which are derived using a two-step procedure from the microscopic Hamiltonian containing one p_z and three σ orbitals per site of the 18-atom unit cell with the hoppings t_i $(i = 1,2,3)$ and V_j $(j = 1,\ldots,9)$ shown in Figs. 1(a) and 1(c). Here, $\tilde{T} \equiv t_2/(TV_2V_3)$, with T defined below Eq. (1).

	Microscopic parameters
$\lambda_{\mathrm{R,int}}$	$-\tilde{T}[2t_3V_3(\sqrt{2}\xi_{p2}\xi_{sp1}+\xi_{p1}\xi_{sp2})+\sqrt{6}t_2V_2\xi_{p1}\xi_{sp1}]/\sqrt{6}$
$\lambda_{\mathrm{R,ext}}$	$2\sqrt{2}t_3^2\xi_{p2}\xi_{sp2}/(3TV_1)$
$\lambda_{\mathrm{I,int}}$	$\sqrt{3}V_6t_2^2\xi_{p1}^2/(4TV_2^2)$
$\lambda_{\mathrm{I,ext}}$	$-t_2t_3V_5\xi_{p1}\xi_{p2}/(2TV_1V_2)$

yield $\lambda_{\mathrm{R,int}}/\lambda_{\mathrm{R,ext}} \approx 5.1$. Using the TB Hamiltonian in Eq. (4) for $\lambda_{I,a} = 0, \lambda_{\mathrm{R,ext}} = 0$, and small values of the internal Rashba SOC parameters, we find that each of the six symmetry-related spin-degenerate Dirac cones at the Γ-M lines splits into a pair perpendicular to this line [Fig. 2(a)]. As this coupling is increased, the pair moves towards the edge of the BZ [Fig. 2(b)], eventually annihilates at the line connecting the K and K' points with another pair, and a topologically trivial gap then opens up [Fig. 2(c)]. Furthermore, at an intermediate value of $\lambda_{\mathrm{R,int}}$ we find that a new pair of Dirac cones emerges, but in this case along the Γ-M line [Fig. 2(d)]. It should be stressed that the order of these Lifshitz phase transitions depends on the precise value of the ratio of the hoppings $t_{\mathrm{ext}}/t_{\mathrm{int}}$. For instance, when its absolute value is slightly larger than 1.18, the pairs on the Γ-M line emerge *before* the other pairs annihilate, and, as $\lambda_{\mathrm{R,int}}$ is further increased, only the former survive (not displayed). In fact, as shown in Figs. 2(e)–2(h), the external Rashba SOC alone creates precisely the effect previously described, therefore opening up the possibility to control the Lifshitz phase transitions with either of the two types of Rashba SOC allowed here.

Effects of the instrinsic SOC: High-Chern-number bands. The intrinsic SOC leads to the formation of topologically nontrivial electronic bands in the system. In β-graphyne internal and external intrinsic SOCs turn out to have the opposite sign (Table I), which results in the enhancement of the topological band gaps as compared to the case when only one of the couplings is present. This can be readily understood from the fact that this sign difference in the six-site effective model arises after integrating out the high-energy orbitals at the edges in the 18-site TB model, which contains both terms with the same sign. Therefore, we will here only consider the effect of the internal intrinsic SOC effectively described by the hopping within the unit cell, $\lambda_{\mathrm{I,int}}$ in Hamiltonian (6). For an infinitesimal value of this coupling, topologically nontrivial bands arise with the corresponding total Chern number at half filling $C_\uparrow = 3$ for spin-up electrons [Fig. 3(a)], as opposed to graphene, where the intrinsic SOC produces $C_\uparrow = 1$. This value of the total Chern number in β-graphyne is a result of the following values of Chern numbers for the six bands $\{-1,2,2,-2,-2,1\}$ [28]. Since the $\mathbb{Z}_2$ invariant is given by the parity of the spin Chern number, $\nu = C_\uparrow \pmod 2$, β-graphyne is a topologically nontrivial insulator. On the other hand, when TRS is broken, for instance by a magnetic field, the system turns into a Chern insulator with Chern number $C = 3$, implying that the Hall conductivity $\sigma_{\mathrm{Hall}} = 3e^2/h$, which differs from graphene where under the same circumstances $\sigma_{\mathrm{Hall}} = e^2/h$. We notice here in passing that β-graphyne cannot become a topological crystalline insulator, since it possesses time-reversal invariant momenta only at the Γ and three symmetry-related M points in the BZ [31]. Furthermore, at a critical value $\lambda_{\mathrm{I,int}}^{\mathrm{crit}} = 0.46$ eV, the band gap at the Fermi level closes at the Γ-K line [Fig. 3(b)] and reopens yielding the Chern numbers $\{-1,2,-4,4,-2,1\}$, and $C_\uparrow = -3$ [Fig. 3(c)]. In addition, for even stronger internal intrinsic SOC, $\lambda_{\mathrm{I,int}} = 0.6$ eV, the band gap closes at the K and K' points [Fig. 3(d)], and upon further increase of this coupling the system enters a topologically nontrivial insulating state with Chern numbers $\{-1,2,-2,2,-2,1\}$ [Fig. 3(e)]. Finally, for $\lambda_{\mathrm{I,int}} = 0.74$ eV, the band gap closes at the Γ point [Fig. 3(f)], and for even stronger $\lambda_{\mathrm{I,int}}$ an insulator with Chern numbers $\{-1,1,-1,1,-1,1\}$ appears.

Discussion and conclusions. To summarize, we here demonstrated that β-graphyne exhibits rich behavior due to the conspiracy of its lattice structure with a relatively large unit cell and the effects of the intrinsic and Rashba SOCs. The latter interaction allows for the tuning of the position and the number of Dirac cones in the band structure therefore opening up the possibility to manipulate the transport properties of the system. Furthermore, we showed that in β-graphyne the Dirac cones can be located at all high-symmetry points in the BZ and a plethora of Lifshitz phase transitions between semimetallic phases can be implemented. Finally, recent progress in realizing honeycomb optical lattices exhibiting tunable Dirac cones [32], in conjunction with the possibility to manipulate SOC in these systems [33], make our findings relevant also for ultracold atoms in optical lattices.

Not only the Rashba SOC induces interesting effects, but the intrinsic SOC also does so. Indeed, the latter yields topologically nontrivial bands, some of which possess high Chern number. Moreover, when TRS is broken and the SOC is tuned, e.g., by the presence of heavy adatoms such as Bi and Sn, a series of topological phase transitions between different Chern insulators is expected to occur. However, further *ab initio* studies are needed to quantitatively establish the effect of adatoms on the SOC in graphynes. The topological band gap closings are at Γ, M, K as well as at points in between, and this system therefore may interpolate between graphene where topological phase transitions occur at the K and K' points [2], and HgTe quantum wells with the topological band gap closing at the Γ point [34–36]. Furthermore, the interplay of SOC and magnetic field (or any TRS-breaking perturbation) is a rich and fundamentally important problem, as the studies in graphene [37] and silicene [38] have shown. Finally, we hope that our results will boost *ab initio* studies of the spin-orbit effects in the graphyne family of carbon allotropes.

Acknowledgments. We would like to thank Douglas S. Galvão for fruitful discussions. This work is part of the D-ITP consortium, a program of the Netherlands Organization for Scientific Research (NWO) that is funded by the Dutch Ministry of Education, Culture, and Science (OCW). The authors acknowledge financial support from NWO.

[1] A. H. Castro Neto, F. Guinea, N. M. R. Peres, K. S. Novoselov, and A. K. Geim, Rev. Mod. Phys. **81**, 109 (2009).
[2] C. L. Kane and E. J. Mele, Phys. Rev. Lett. **95**, 146802 (2005).
[3] E. Kalesaki, C. Delerue, C. Morais Smith, W. Beugeling, G. Allan, and D. Vanmaekelbergh, Phys. Rev. X **4**, 011010 (2014).
[4] M. Gibertini, A. Singha, V. Pellegrini, M. Polini, G. Vignale, A. Pinczuk, L. N. Pfeiffer, and K. W. West, Phys. Rev. B **79**, 241406 (2009).
[5] K. K. Gomes, W. Mar, W. Ko, F. Guinea, and H. C. Manoharan, Nature (London) **483**, 306 (2012).
[6] Y. Li, L. Xu, H. Liu, and Y. Li, Chem. Soc. Rev. **43**, 2572 (2014).
[7] G. X. Li, Y. L. Li, H. B. Liu, Y. B. Guo, Y. J. Li, and D. B. Zhu, Chem. Commun. **46**, 3256 (2010).
[8] F. Diedrich and M. Kivale, Adv. Mater. **22**, 803 (2010).
[9] P. Rivera Fuentes and F. Diedrich, Angew. Chem., Int. Ed. **51**, 2818 (2012).
[10] R. H. Baughman, H. Eckhardt, and M. Kertesz, J. Chem. Phys. **87**, 6687 (1987).
[11] N. Narita, S. Nagai, S. Suzuki, and K. Nakao, Phys. Rev. B **58**, 11009 (1998).
[12] V. R. Coluci, S. F. Braga, S. B. Legoas, D. S. Galvão, and R. H. Baughman, Phys. Rev. B **68**, 035430 (2003).
[13] K. Tahara, T. Yoshimura, M. Sonoda, Y. Tobe, and R. V. Williams, J. Org. Chem. **72**, 1437 (2007).
[14] J. Kang, J. Li, F. Wu, S.-S. Li, and J.-B. Xia, J. Phys. Chem. C **115**, 20466 (2011).
[15] Q. Yue, S. Chang, J. Kang, J. Tan, S. Qin, and J. Li, J. Chem. Phys. **136**, 244702 (2012).
[16] S. W. Cranford and M. J. Buehler, Carbon **49**, 4111 (2011).
[17] B. G. Kim and H. J. Choi, Phys. Rev. B **86**, 115435 (2012).
[18] D. Malko, C. Neiss, F. Vines, and A. Görling, Phys. Rev. Lett. **108**, 086804 (2012).
[19] H. Huang, W. Duan, and Z. Liu, New J. Phys. **15**, 023004 (2013).
[20] J.-J. Zheng, X. Zhao, Y. Zhao, and X. Gao, Sci. Rep. **3**, 1271 (2013).
[21] J.-J. Zheng, X. Zhao, S. B. Zhang, and X. Gao, J. Chem. Phys. **138**, 244708 (2013).
[22] J. He, S. Y. Ma, P. Zhou, C. X. Zhang, C. He, and L. Z. Sun, J. Phys. Chem. C **116**, 26313 (2012).
[23] K. F. Garrity and D. Vanderbilt, Phys. Rev. Lett. **110**, 116802 (2013).
[24] C. Weeks, J. Hu, J. Alicea, M. Franz, and R. Wu, Phys. Rev. X **1**, 021001 (2011).
[25] M. Zhao, W. Dong, and A. Wang, Sci. Rep. **3**, 3532 (2013).
[26] S. A. Parameswaran, R. Roy, and S. L. Sondhi, C. R. Physique **14**, 816 (2013).
[27] Z. Liu, G. Yu, H. Yao, L. Liu, L. Jiang, and Y. Zheng, New J. Phys. **14**, 113007 (2012).
[28] See Supplemental Material at http://link.aps.org/supplemental/10.1103/PhysRevB.90.081406 for derivation of the effective Hamiltonians and the calculation of Chern numbers.
[29] S. Konschuh, M. Gmitra, and J. Fabian, Phys. Rev. B **82**, 245412 (2010).
[30] For a discussion on the effects of SOC arising from the *d* orbitals in graphynes, see G. van Miert, V. Juričić, and C. Morais Smith (unpublished).
[31] R.-J. Slager, A. Mesaros, V. Juričić, and J. Zaanen, Nat. Phys. **9**, 98 (2013).
[32] L. Tarruell, D. Greif, T. Uehlinger, G. Jotzu, and T. Esslinger, Nature (London) **483**, 302 (2012).
[33] V. Galitski and I. B. Spielman, Nature (London) **494**, 49 (2013).
[34] B. A. Bernevig, T. A. Hughes, and S. C. Zhang, Science **314**, 1757 (2006).
[35] M. König, S. Wiedmann, C. Brüne, A. Roth, H. Buhmann, L. W. Molenkamp, X.-L. Qi, and S.-C. Zhang, Science **318**, 766 (2007).
[36] W. Beugeling, E. Kalesaki, C. Delerue, Y.-M. Niquet, D. Vanmaekelbergh, and C. Morais Smith (unpublished).
[37] W. Beugeling, N. Goldman, and C. M. Smith, Phys. Rev. B **86**, 075118 (2012).
[38] M. Ezawa, Y. Tanaka, and N. Nagaosa, Sci. Rep. **3**, 2790 (2014).